Synthesis, Characterization, and Electrocatalytic Activity toward Methanol Oxidation of Carbon-Supported Ptx–(RuO2–M)1–x Composite Ternary Catalysts (M = CeO2, MoO3, or PbOx)

ARTICLE *in* ENERGY & FUELS · JUNE 2010

Impact Factor: 2.79 · DOI: 10.1021/ef100424m

Energy Fuels **XXXX**, *XXX*, 000–000 · DOI:10.1021/ef100424m

energy&fuels
article

Synthesis, Characterization, and Electrocatalytic Activity toward Methanol Oxidation of Carbon-Supported $Pt_x-(RuO_2-M)_{1-x}$ Composite Ternary Catalysts (M = CeO_2, MoO_3, or PbO_x)

Katlin I. B. Eguiluz,*[,†] Geoffroy R. P. Malpass,[‡] Marilia M. S. Pupo,[†] Giancarlo R. Salazar-Banda,[†] and Luis A. Avaca[§]

[†]*Instituto de Tecnologia e Pesquisa/Programa de Pós-Graduação em Engenharia de Processos, Universidade Tiradentes, Aracaju, Sergipe (SE), 49032-490 Brazil,* [‡]*Universidade Federal do ABC, Santo André, São Paulo (SP), 09210-170, Brazil, and* [§]*Instituto de Química de São Carlos, Universidade de São Paulo, CP 780, São Carlos, São Paulo (SP), 13560-970, Brazil*

Received April 5, 2010. Revised Manuscript Received June 7, 2010

Carbon-supported platinum is commonly used as an anode electrocatalyst in low-temperature fuel cells fueled with methanol. The cost of Pt and the limited world supply are significant barriers for the widespread use of this type of fuel cell. Moreover, Pt used as anode material is readily poisoned by carbon monoxide produced as a byproduct of the alcohol oxidation. Although improvements in the catalytic performance for methanol oxidation were attained using Pt−Ru alloys, the state-of-the-art Pt−Ru catalyst needs further improvement because of relatively low catalytic activity and the high cost of noble Pt and Ru. For these reasons, the development of highly efficient ternary platinum-based catalysts is an important challenge. Thus, various compositions of ternary $Pt_x-(RuO_2-M)_{1-x}/C$ composites (M = CeO_2, MoO_3, or PbO_x) were developed and further investigated as catalysts for the methanol electro-oxidation reaction. The characterization carried out by X-ray diffraction, energy-dispersive X-ray analysis, transmission electron microscopy, X-ray photoelectron spectroscopy, and cyclic voltammetry point out that the different metallic oxides were successfully deposited on the Pt/C, producing small and well-controlled nanoparticles in the range of 2.8−4.2 nm. Electrochemical experiments demonstrated that the $Pt_{0.50}(RuO_2-CeO_2)_{0.50}/C$ composite displays the higher catalytic activity toward the methanol oxidation reaction (lowest onset potential of 207 mV and current densities taken at 450 mV, which are 140 times higher than those at commercial Pt/C), followed by the $Pt_{0.75}(RuO_2-MoO_3)_{0.25}/C$ composite. In addition, both of these composites produced low quantities of formic acid and formaldehyde when compared to a commercially available $Pt_{0.75}-Ru_{0.25}/C$ composite (from E-Tek, Inc.), suggesting that the oxidation of methanol occurs mainly by a pathway that produces CO_2 forming the intermediary CO_{ads}.

1. Introduction

The development of new materials that can solve challenging problems in the areas of clean energy production and conversion is of paramount importance in the quest to find an alternative to environmentally unfriendly fossil-fuel use. A promising alternative is the polymer electrolyte membrane fuel cells (PEMFCs).[1−3] Fuel cells can be viewed as devices for electrochemically converting chemical fuels into electricity. They offer extremely high chemical−electrical conversion efficiencies because of the absence of the Carnot limitation. Furthermore, the technology does not produce significant amounts of pollutants, such as nitrogen oxides, especially when compared to internal-combustion engines. As a result, there is now a phenomenal commercial interest in fuel-cell technology, with new start-up companies being established and major players in the energy market turning their attention to it. The degree and extent of market penetration and establishment really only depend upon the ability to reduce the cost of these devices while ensuring their long-term stability.

Among the PEMFC systems, direct methanol fuel cells (DMFCs), using liquid and renewable methanol fuel, have been considered to be a good option in terms of fuel usage and feed strategies.[4,5] In comparison to hydrogen-fed fuel cells, which have a reforming unit or low capacity in the hydrogen storage tank, DMFC uses a liquid methanol fuel, which is easily stored and transported and simplifies the fuel-cell system. It has been recognized that the success of fuel-cell technology partially depends upon the electrode performance.

In DMFCs, the slow anode kinetics can only be overcome by developing new anode catalysts. For performance improvement of the DMFC anode catalyst, the investigation of new catalytic materials, including noble and non-noble metals, is necessary. Traditionally, for a pure platinum catalyst, the adsorption of CO, one of the intermediates in methanol electro-oxidation, can occupy the reaction active sites, resulting in slow reaction kinetics. Besides, the formation of oxygen-containing species (mainly OH) by water activation on the Pt surface, which is a necessary step for the oxidative removal of adsorbed CO, requires a high over potential. When a second metal, such as ruthenium, alloys with platinum, the oxidation kinetic of

*To whom correspondence should be addressed. Telephone: +55-79-32182190 ext. 2548. Fax: +55-79-32182190. E-mail: katlinbarrios@gmail.com.

(1) Dresselhause, M. S.; Thomas, I. L. *Nature* **2001**, *414*, 332–337.
(2) Steele, B. C. H.; Heinzel, A. *Nature* **2001**, *414*, 354–352.
(3) Markovic, N. M.; Ross, P. N. *Surf. Sci. Rep.* **2002**, *45*, 117–230.
(4) Wasmus, S.; Kuver, A. *J. Electroanal. Chem.* **1999**, *461*, 14–31.
(5) Arico, A. S.; Srinivasan, S.; Antonucci, V. *Fuel Cells* **2001**, *2*, 133–161.

methanol is improved significantly, reaching a practicable level. Thus, the use of a second metal that can provide oxygenated species at lower potentials for oxidative removal of adsorbed CO is certainly needed (bifunctional mechanism). Among binary Pt-based alloys, Pt−Ru has been found to be the most active binary catalyst and is the state-of-the-art anode catalyst for DMFCs.

Ternary Pt alloys offer the potential to increment the catalyst activity compared to single or bimetallic systems. This is because surface or sub-surface atoms of additional metals result in modifications of the electronic or structural characteristics of the single or bimetallic alloy surface.[6] Ternary Pt−Ru−Fe,[7] Pt−Ru−Ni,[8] Pt−Ru−Co,[9] Pt−Ru−W,[10] and Pt−Ru−Ir[11] have been reported as highly active catalysts for methanol oxidation.

Recent studies using catalysts with transition-metal oxides and rare earth oxides[12−14] have shown that these can improve electrocatalytic properties in the methanol oxidation reaction. CeO_2 is one of the most interesting industrial oxides because oxygen vacancy defects can be rapidly formed and eliminated in its presence, giving it a high "oxygen storage capacity". It is this capacity that makes modern automotive exhaust treatment catalysts containing CeO_2 much more effective than their predecessors without CeO_2. Thus, enhanced catalytic activity toward methanol oxidation was already observed on Pt/CeO_2 composites.[12,13]

Furthermore, the addition of molybdenum on Pt[15−19] and Pt−Ru[20−23] catalysts has attracted major attention in recent years. Studies of CO oxidation on polycrystalline PtMo alloys indicate that the conventional bifunctional mechanism is responsible for the CO tolerance of these materials.[24] Water-induced oxide formation has been attributed to Mo,[25] which shows high water dissociation capability. Moreover, intermetallic PtPb was recently shown to be resistant to CO poisoning when formic acid is used as a fuel,[26] whereas a pure Pt surface poisons immediately.[16] In addition, it has been recently reported that the catalysts $Pt-PbO_x$ and $Pt-(RuO_2-PbO_x)$ with 10% of catalyst load exhibited significantly enhanced catalytic activity toward the methanol oxidation reaction as compared to $Pt-(RuO_2)/C$ and Pt/C electrodes.[27]

On the other hand, among the methods for the preparation of high-area composite catalysts, the sol−gel method has proven to be a simple, efficient, and very appropriate technique to produce nanometric catalytic deposits with the desired composition on powder surfaces[11,27−32] and solid substrates[33−36] at a low cost. The sol−gel technology offers other important advantages, such as low life-cycle environmental impact and simple application procedures easily adaptable within the industry, and also facilitates the combination of materials.

Considering the importance of a ternary Pt-containing catalyst for the development of new materials with high catalytic activity toward methanol oxidation, this study describes the preparation of ternary composites containing $Pt_x-(RuO_2-M)_{1-x}/C$ (where M represent CeO_2, MoO_3, or PbO_x) by the sol−gel method from Pt/C (from E-Tek, Inc.) commercial catalysts. Thus, the effect of catalyst composition on the methanol electro-oxidation in acid media was studied using cyclic voltammetry, quasi-steady-state polarization curves (Tafel plots), and chronoamperometric tests. The developed composite catalysts were characterized by X-ray diffraction (XRD), energy-dispersive X-ray analysis (EDX), transmission electron microscopy (TEM), X-ray photoelectron spectroscopy (XPS), and cyclic voltammetry (CV). In addition, the catalytic performance of the composite electrodes prepared in this study was compared among themselves and to that obtained for commercially available Pt/C and $Pt_{0.75}-Ru_{0.25}/C$ catalytic powders using electrochemical experiments.

2. Experimental Section

2.1. Catalyst Preparation. The catalysts were prepared by the sol−gel method using a commercial Pt/C (from E-Tek, Inc.) powder containing 10% platinum as a substrate. The co-catalyst was deposited by dissolving the metallic precursors (ruthenium acetylacetonate and lead acetylacetonate, molybdenum acetate dimer, or ceric ammonium nitrate, all from Aldrich) in a solvent containing isopropanol and acetic acid 3:2 (v/v). After that, an appropriate amount of Pt/C was added to the resulting sol and the mixture was homogenized by ultrasonic irradiation (20 kHz) produced by a Heat System Ultrasonic W85 sonicator for 30 min.

(6) Stamenkovic, V.; Moon, B. S.; Mayerhofer, K. J.; Ross, P. N.; Markovic, N.; Rossmeisl, J.; Greeley, J.; Norskov, J. K. *Angew. Chem., Int. Ed.* **2006**, *45*, 2897–2901.
(7) Jeon, M. K.; Lee, K. R.; Daimon, H.; Nakahara, A.; Woo, S. I. *Catal. Today* **2008**, *132*, 123–126.
(8) Liu, J.; Cao, J.; Huang, Q.; Li, X.; Zou, Z.; Yang, H. *J. Power Sources* **2008**, *175*, 159–165.
(9) Strasser, P. *J. Comb. Chem.* **2008**, *10*, 216–224.
(10) Cooper, J. S.; McGinn, P. J. *J. Power Sources* **2006**, *163*, 330–338.
(11) Eguiluz, K. I. B.; Salazar-Banda, G. R.; Miwa, D.; Machado, S. A. S.; Avaca, L. A. *J. Power Sources* **2008**, *179*, 42–49.
(12) Bai, Y.; Wu, J.; Qiu, X.; Xi, J.; Wang, J.; Li, J.; Zhu, W.; Chen, L. *Appl. Catal., B* **2007**, *73* (1−2), 144–149.
(13) Díaz, D. J.; Greenletch, N.; Solanki, A.; Karakoti, A.; Seal, S. *Catal. Lett.* **2007**, *119*, 319–326.
(14) Lim, D.; Lee, W.; Choi, D.; Kwon, H.; Lee, H. *Electrochem. Commun.* **2008**, *10*, 592–596.
(15) Santiago, E. I.; Batista, M. S.; Assaf, E. M.; Ticianelli, E. A. *J. Electrochem. Soc.* **2004**, *151*, A944.
(16) Mylswamy, S.; Wang, C. Y.; Liu, R. S.; Lee, J. F.; Tang, M. J.; Lee, J. J.; Weng, B. J. *Chem. Phys. Lett.* **2005**, *412*, 444–488.
(17) Ordonez, L. C.; Roquero, P.; Sebastian, P. J.; Ramirez, J. *Catal. Today* **2005**, *46*, 107–108.
(18) Lebedeva, N. P.; Janssen, G. J. M. *Electrochim. Acta* **2005**, *51*, 29–40.
(19) Ioroi, T.; Akita, T.; Yamazaki, S. I.; Siroma, Z.; Fujiwara, N.; Yasuda, K. *Electrochim. Acta* **2006**, *52*, 491–498.
(20) Oliveira Neto, A.; Franco, E. G.; Arico, E.; Linardi, M.; Gonzalez, E. R. *J. Eur. Ceram. Soc.* **2003**, *23*, 2987–2992.
(21) Zhang, X.; Zhang, F.; Chan, K. Y. *J. Mater. Sci.* **2004**, *39*, 5845–5848.
(22) Song, C. J.; Khanfar, M.; Pickup, P. G. *J. Appl. Electrochem.* **2006**, *36*, 339–345.
(23) Benker, N.; Roth, C.; Mazurek, M.; Fuess, H. *J. New Mater. Electrochem. Syst.* **2006**, *9*, 121–126.
(24) Grgur, B. N.; Markovic, N. M.; Ross, P. N., Jr. *J. Phys. Chem. B* **1998**, *102*, 2494–2501.
(25) Anderson, A. B.; Grantscharova, E.; Seong, S. *J. Electrochem. Soc.* **1996**, *143*, 2075–2072.
(26) Casado-Rivera, E.; Volpe, D. J.; Alden, L.; Lind, C.; Downie, C.; Vazquez-Alvarez, T.; Angelo, A. C. D.; DiSalvo, F. J.; Abruna, H. D. *J. Am. Chem. Soc.* **2004**, *126*, 4043–4049.
(27) Suffredini, H. B.; Salazar-Banda, G. R.; Avaca, L. A. *J. Sol-Gel Sci. Technol.* **2008**, *49*, 131–136.
(28) Suffredini, H. B.; Tricoli, V.; Avaca, L. A.; Vatistas, N. *Electrochem. Commun.* **2004**, *6*, 1025–1028.
(29) Suffredini, H. B.; Tricoli, V.; Vatistas, N.; Avaca, L. A. *J. Power Sources* **2006**, *158*, 124–128.
(30) Calegaro, M. L.; Suffredini, H. B.; Machado, S. A. S.; Avaca, L. A. *J. Power Sources* **2006**, *156*, 300–305.
(31) Salazar-Banda, G. R.; Eguiluz, K. I. B.; Avaca, L. A. *Electrochem. Commun.* **2007**, *9*, 59–64.
(32) Suffredini, H. B.; Salazar-Banda, G. R.; Avaca, L. A. *J. Power Sources* **2007**, *171*, 355–362.
(33) Salazar-Banda, G. R.; Suffredini, H. B.; Avaca, L. A. *J. Braz. Chem. Soc.* **2005**, *16*, 903.
(34) Suffredini, H. B.; Salazar-Banda, G. R.; Tanimoto, S. T.; Calegaro, M. L.; Machado, S. A. S.; Avaca, L. A. *J. Braz. Chem. Soc.* **2006**, *17*, 257.
(35) Salazar-Banda, G. R.; Suffredini, H. B.; Calegaro, M. L.; Tanimoto, S. T.; Avaca, L. A. *J. Power Sources* **2006**, *162*, 9–20.
(36) Salazar-Banda, G. R.; Suffredini, H. B.; Avaca, L. A.; Machado, S. A. S. *Mater. Chem. Phys.* **2009**, *117*, 434–442.

The solvent was then slowly evaporated at ~70 °C, and the resulting powder was submitted to a thermal treatment at 400 °C in an inert argon atmosphere for 60 min, using a heating rate of 5 °C/min. After the thermal treatment was completed, the oven was turned off to reduce the temperature until atmospheric temperature was reached.

The desired amounts of modifiers were calculated in relation to the amount of platinum in the catalytic powder. Approximately 0.25 g of each catalytic composite was prepared. The ternary composites were prepared having a fixed atomic relation between the elements Ru and M (M = Pb, Mo, or Ce) of 1:1 and varying the atomic relation between Pt and the mixture of Ru and the third element. The ternary composites are arranged in three groups: (i) $Pt_{0.25}(RuO_2-CeO_2)_{0.75}/C$, $Pt_{0.50}(RuO_2-CeO_2)_{0.50}/C$, and $Pt_{0.75}(RuO_2-CeO_2)_{0.25}/C$; (ii) $(PtO_x)_{0.25}(RuO_2-PbO_x)_{0.75}/C$, $(PtO_x)_{0.50}(RuO_2-PbO_x)_{0.50}/C$, and $(PtO_x)_{0.75}(RuO_2-PbO_x)_{0.25}/C$; and (iii) $Pt_{0.25}(RuO_2-MoO_3)_{0.75}/C$, $Pt_{0.50}(RuO_2-MoO_3)_{0.50}/C$, and $Pt_{0.75}(RuO_2-MoO_3)_{0.25}/C$.

For comparison, some experiments were also carried out using Pt/C and $Pt_{0.75}-Ru_{0.25}/C$ commercially available catalytic composites from E-Tek, Inc.

2.2. Electrochemical Experiments. The working electrodes were constructed using the thin porous coating (TPC) configuration.[37] A pyrolitic graphite rod (ϕ = 5 mm) inserted in a Teflon cylinder and leaving a small cavity (≈0.3 mm) at the end was used to support the catalysts. The working electrodes were prepared by placing ~10 mg of the catalyst/carbon mixture in a small beaker with ultrapure water under ultrasonic agitation for about 5 min. Subsequently, a dilute suspension of a Teflon emulsion (du Pont T30B, 60% Teflon in water plus 7% Triton X-100 as a stabilizer) was added to the dispersion to yield ~10% (w/w) of Teflon in the final dry solid material. The mixture was filtered through a 0.45-μm Millipore membrane, kneaded with a spatula onto a glass slide, and about 0.5 ± 0.1 mg based on dry weight was applied into the shallow disk cavity (≈0.3 mm deep) of a rotating pyrolytic graphite disk electrode. The surface of this porous carbon coating was smoothened using a spatula to create a common plane with the front of the electrode assembly. Any material that may have been accidentally spread onto the gap, ring, or remainder of the mounting was carefully removed with a soft lens paper.

All electrochemical measurements were carried out using the TPC electrode configuration. A three-electrode two-compartment Pyrex glass cell was used for the electrochemical measurements. The counter electrode was a 2 cm^2 platinum foil, and the reference electrode was a hydrogen electrode in the same solution (HESS) that was connected by a Luggin capillary. All of the experiments were carried out at room temperature in a 0.5 M H_2SO_4 (Merck) aqueous solution also containing 0.5 M methanol (J.T. Baker). Sulfuric acid is used as an electrolyte considering that sulfonated Nafion (a sulfuric acid in a solid polymer form)-based membranes are typically used as the polymer electrolyte membranes in fuel cells. The solutions were prepared with analytical-grade reagents without further purification, and water was supplied by a Milli-Q system from Millipore, Inc. and was N_2-saturated prior to the measurements.

The electrochemical experiments were carried out using an Autolab model PGSTAT 30 potentiostat/galvanostat coupled to an IBM-PC compatible microcomputer. All cyclic voltammetric curves reported here correspond to the stationary responses obtained for electrodes cycled between 50 and 1100 mV versus HESS. The quasi-steady-state polarization curves were carried out in the potentiostatic mode, with all data points obtained after 300 s of polarization at each potential.

2.3. Catalyst Characterization. The physical characterization of the catalysts was initially performed by XRD in a universal diffractometer Carl Zeiss-Jena, URD-6, operating with Cu Kα radiation (λ = 0.154 06 nm) generated at 50 kV and 100 mA. The scans were carried out at 1° min^{-1} for 2θ values between 5° and 100°. This was followed by EDX measurements in a LEO model 440 spectrophotometer with a silicon−lithium detector having a Be window and applying 113 eV. The XRD patterns were also analyzed by the software Winfit 1.2 to determine the mean size of the catalyst crystallites.[38] In addition, TEM images were taken using a Philips CM200 microscope operating at 200 kV, coupled to a high-resolution energy-dispersive X-ray analysis spectrometer detector EDX Princeton Gamma Tech PGT Prism. The samples for the TEM and high-resolution EDX analyses were prepared by ultrasonically dispersing the catalyst powders in ethanol. A drop of the suspension was applied to a carbon-coated copper grid and was dried in air. Samples studied by EDX coupled to a MEV apparatus were prepared by fixing a proper amount of the catalyst powders onto an aluminum substrate using a conducting tape and scanning a ~0.5 cm^2 area every time.

X-ray photoelectron spectroscopy spectra of the prepared composites were acquired at room temperature using a commercial spectrometer (VG-Escalab). The Al Kα line was used ($h\nu$ = 1486.6 eV), and the analyzer pass energy was set to 10 eV. All of the binding energies were corrected using the signal of the main peak of hydrocarbon component (C 1s line) of adventitious carbon at 285.0 eV as an internal standard. The elastic backgrounds of the different core-level spectra were subtracted using Shirley's method. No additional treatment was applied to the samples prior to these measurements.

3. Results

3.1. Characterization of the Composites. Photoelectron spectroscopy analyses were used to determinate the oxidation state of the elements on the catalyst surfaces. This information must be interpreted by taking into account its limitations because the oxidation state of catalysts probably changes during the electrochemical process. Figure 1 shows the complete spectra of three composites, each one of a studied group [$Pt_{0.75}(RuO_2-MoO_3)_{0.25}/C$, $Pt_{0.50}(RuO_2-CeO_2)_{0.50}/C$, and $(PtO_x)_{0.25}(RuO_2-PbO_x)_{0.75}/C$], which are representative of the total of ternary composites. These spectra reveal the existence of C, O, Pt, and the other metals from the different composites (Ru, Mo, Ce, and/or Pb).

The spectrum of Figure 2A taken on the $Pt_{0.75}(RuO_2-MoO_3)_{0.25}/C$ composite displays two peaks of the Pt 4f ($4f_{7/2}$ and $4f_{5/2}$). These signals can be deconvoluted in three components in 71.6 and 74.9 eV (component 1), 72.9 and 76.2 eV (component 2), and 75.0 and 77.6 eV (component 3), which correspond, respectively,[39] to the oxidation states of platinum, 0, 2+, and 4+, with a metallic platinum content of about 65%.

The peak positions, the peak assignments, and the relative concentration are summarized in Table 1. Similarly, both the XPS spectrum and relative composition for the Pt 4f were observed on the $Pt_{0.50}(RuO_2-CeO_2)_{0.50}/C$ composite (not shown). However, the relative composition of the oxidation states of platinum were different on the $(PtO_x)_{0.25}(RuO_2-PbO_x)_{0.75}/C$ system (Figure 2G), where the metal undergoes a higher oxidation. The quantitative analysis of this composite results in 50% metallic Pt and 50% oxidized Pt as Pt^{2+} [probably PtO or $Pt(OH)_2$, ~34%] and Pt^{4+} (probably PtO_2, ~16%). As a result, in the composites containing lead, the platinum was named as PtO_x (x = 0, 2, or 4). The thermal

(37) Tanaka, A. A.; Fierro, C.; Scherson, D.; Yeager, E. B. *J. Phys. Chem.* **1987**, *91*, 3799–3807.

(38) Krumm, S. *Comput. Geosci.* **1999**, *25*, 489–499.

(39) Raman, R. K.; Shukla, A. K.; Gayen, A.; Hegde, M. S.; Priolkar, K. R.; Sarode, P. R.; Emura, S. *J. Power Sources* **2006**, *157*, 45–55.

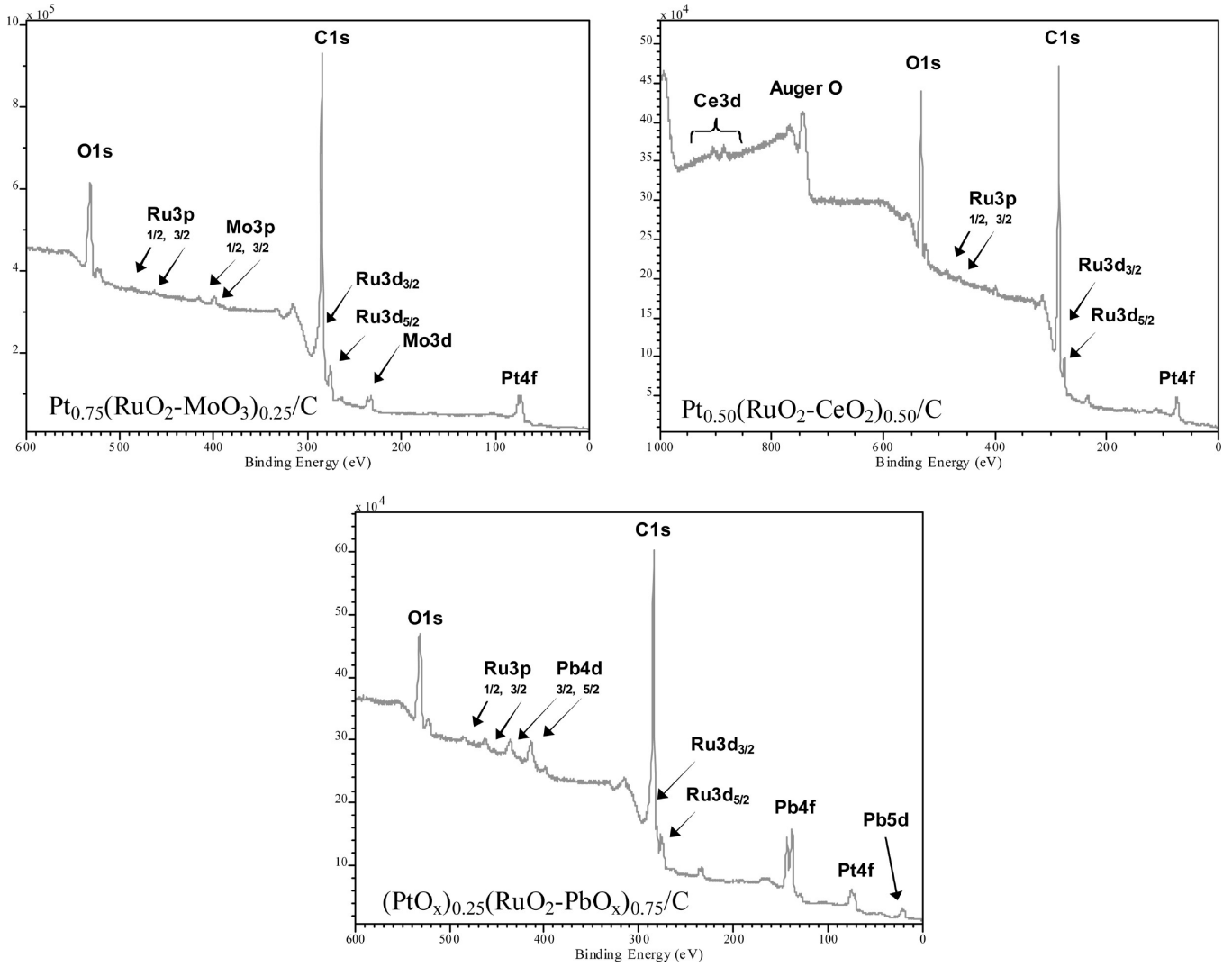

Figure 1. XPS spectrum of the ternary catalysts: $Pt_{0.75}(RuO_2{-}MoO_3)_{0.25}/C$, $Pt_{0.50}(RuO_2{-}CeO_2)_{0.50}/C$, and $(PtO_x)_{0.25}(RuO_2{-}PbO_x)_{0.75}/C$.

treatment used in the sol−gel process for the preparation of the composites could explain the presence of oxidized platinum on the catalysts.

The Ru $3p_{3/2}$ signal (Figure 2C) was used to identify and quantify the oxidation states of ruthenium[40] because of the superposition of the Ru 3d features with the C 1s ones (Figure 2B), where the peaks 1, 2, 3, 4, 5, and 6 correspond to Ru^{4+}, Ru^{6+}, C−C, C−H, C−O, and C═O, respectively. Thus, the feature related to Ru $3p_{3/2}$ can be deconvoluted into two components at 462.1 and 464.6 eV corresponding to Ru^{4+} and Ru^{6+}, respectively (see Table 1). As expected, the preferential deposition of ruthenium oxides was as Ru^{4+} (74%), probably as RuO_2, which is the same oxide composition found in the analyses of the Ru $3d_{5/2}$ and $3d_{3/2}$ features (not shown).

Likewise, Figure 2D shows the deconvolution of Mo $3d_{5/2}$ and $3d_{3/2}$ features.[41] These two pairs of peaks are related to the metallic molybdenum at 228 and 231 eV and Mo^{6+} at 232.5 and 235.6 eV with a preferential deposition in the oxidation state Mo^{6+} (∼84%), most likely as MoO_3, as will be discussed hereafter from XRD analyses.

In the case of the catalysts containing cerium, this element was preferentially deposited in the oxidation state 4+. The deconvoluted pair peaks observed in Figure 2E related to Ce^{4+} are denoted as "v" ($v_0{-}v'_0$ and $v_1{-}v'_1$)[42] in 882.4 and 900.9 and in 887.3 and 906.2 eV, and a peak also corresponds to Ce^{4+} ($3d_{5/2}$) expressed as v_2 in 898.2 eV, whose pair peak ($3d_{3/2}$) should appear at ∼916.1 eV (out of the spectrum scale of Figure 2F). Furthermore, the doublet peaks associated to Ce^{3+} are denoted by the character "u" ($u_0{-}u'_0$) at 885.34 and 903.8 eV.[42] As observed in Table 1, the favored deposition of cerium was as an oxidation state of 4+ (∼67%) likely in the form of CeO_2.

Finally, as displayed in Table 1 and Figure 2H, lead is present as Pb^{2+}, Pb^{4+}, or as a mixture of both states (Pb^{2+} and Pb^{4+}) in Pb_3O_4. These oxidation stages suggest that this element could be deposited as individual oxides PbO and PbO_2 and mainly as a mixture of oxides Pb_3O_4 ($2PbO\cdot PbO_2$), as will be discussed hereafter from XRD experiments. Moreover, any feature of metallic lead was observed by XPS in binding energies of about 137 eV, discarding the deposition of

(40) Salomonsson, A.; Petoral, R. M., Jr.; Uvdal, K.; Aulin, C.; Kall, P.-O.; Ojamäe, L.; Strand, M.; Sanati, M.; Spetz, A. L. *J. Nanopart. Res.* **2006**, *8*, 899–910.

(41) Ramana, C. V.; Atuchin, V. V.; Kesler, V. G.; Kochubey, V. A.; Pokrovsky, L. D.; Shutthanandan, V.; Becker, U.; Ewing, R. C. *Appl. Surf. Sci.* **2007**, *253*, 5368–5374.

(42) Larachi, F.; Pierre, J.; Adnot, A.; Bernis, A. *Appl. Surf. Sci.* **2002**, *195*, 236–250.

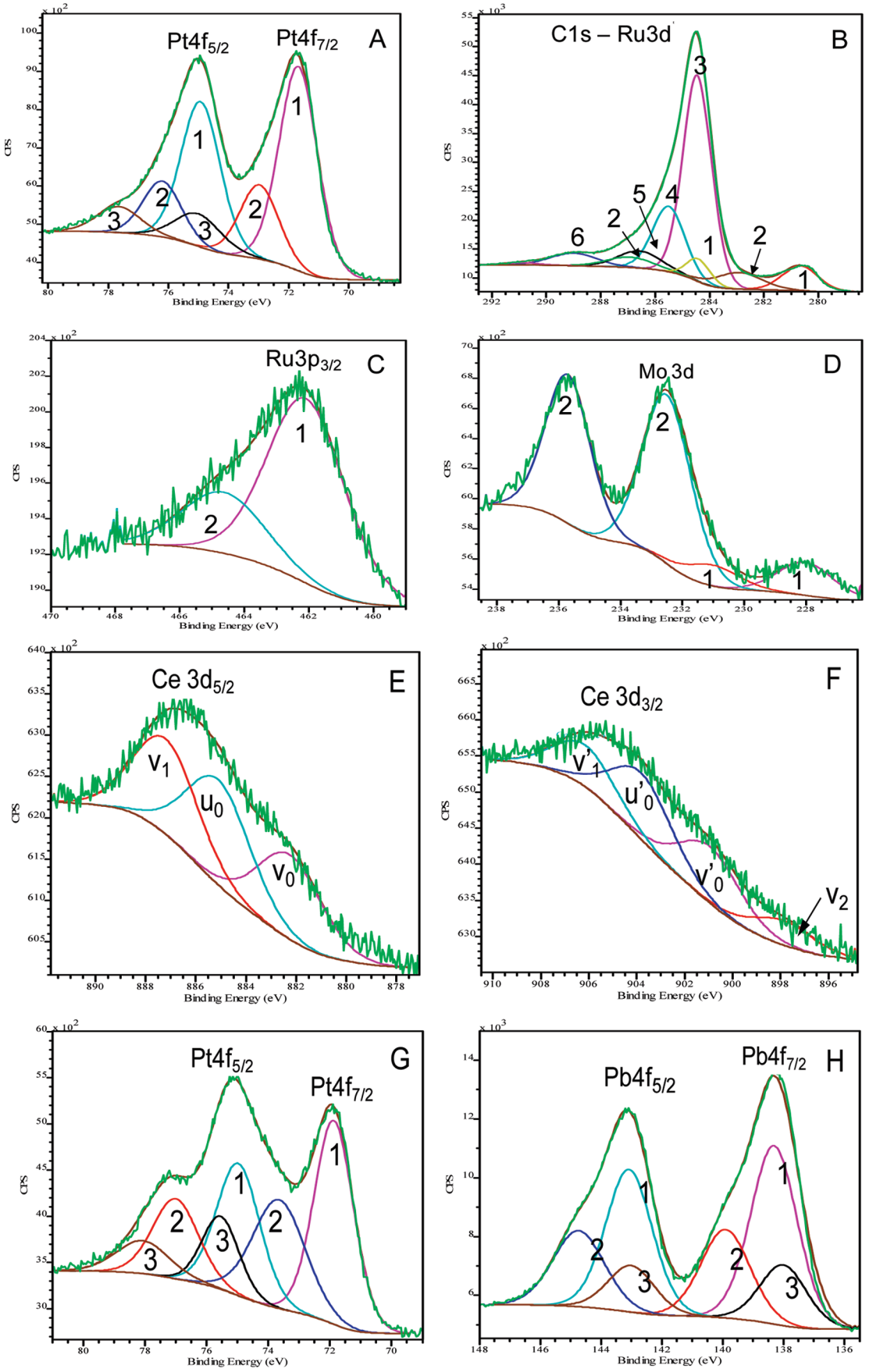

Figure 2. Deconvolution of relative peaks from XPS spectra at (A) Pt 4f, (B) C 1s and Ru 3d, (C) Ru 3p [$Pt_{0.75}(RuO_2-MoO_3)_{0.25}$/C, $Pt_{0.50}(RuO_2-CeO_2)_{0.50}$/C, and $(PtO_x)_{0.25}(RuO_2-PbO_x)_{0.75}$/C], (D) Mo 3d [$Pt_{0.75}(RuO_2-MoO_3)_{0.25}$/C], (E and F) Ce 3d [$Pt_{0.50}(RuO_2-CeO_2)_{0.50}$/C], (G) Pt 4f, and (H) Pb 4f [$(PtO_x)_{0.25}(RuO_2-PbO_x)_{0.75}$/C].

Table 1. Binding Energies and Relative Amounts of the Species Present on the Ternary Composite Catalysts: $Pt_{0.75}(RuO_2-MoO_3)_{0.25}/C$, $Pt_{0.50}(RuO_2-CeO_2)_{0.50}/C$, and $(PtO_x)_{0.25}(RuO_2-PbO_x)_{0.75}/C$, As Exhibited in the First Column

composite catalysts	species	binding energy (eV)	relative percentage (%)
$Pt_{0.75}(RuO_2-MoO_3)_{0.25}/C$ $Pt_{0.50}(RuO_2-CeO_2)_{0.50}/C$	$Pt4f_{7/2}$ (Pt^0)	71.6	37.05
	$Pt4f_{5/2}$ (Pt^0)	74.9	26.93
	$Pt4f_{7/2}$ (Pt^{2+})	72.9	13.54
	$Pt4f_{5/2}$ (Pt^{2+})	76.2	10.09
	$Pt4f_{7/2}$ (Pt^{4+})	75	7.07
	$Pt4f_{5/2}$ (Pt^{4+})	77.6	5.32
$Pt_{0.75}(RuO_2-MoO_3)_{0.25}/C$ $Pt_{0.50}(RuO_2-CeO_2)_{0.50}/C$ $(PtO_x)_{0.25}(RuO_2-PbO_x)_{0.75}/C$	$Ru3p_{3/2}$ (Ru^{4+})	462.1	74.05
	$Ru3p_{3/2}$ (Ru^{6+})	464.6	25.95
$Pt_{0.75}(RuO_2-MoO_3)_{0.25}/C$	Mo $3d_{5/2}$ (Mo)	228.0	10.29
	Mo $3d_{3/2}$ (Mo)	231.0	6.21
	Mo $3d_{5/2}$ (MoO_3)	232.5	46.07
	Mo $3d_{3/2}$ (MoO_3)	235.6	37.44
$Pt_{0.50}(RuO_2-CeO_2)_{0.50}/C$	Ce $3d_{5/2}$ ($v_0 = Ce^{4+}$)	882.4	26.35
	Ce $3d_{5/2}$ ($v_1 = Ce^{4+}$)	887.3	29.46
	Ce $3d_{5/2}$ ($v_2 = Ce^{4+}$)	898.2	11.59
	Ce $3d_{3/2}$ ($v'_0 = Ce^{4+}$)	900.9	34.45
	Ce $3d_{3/2}$ ($v'_1 = Ce^{4+}$)	906.2	25.27
	Ce $3d_{5/2}$ ($u_0 = Ce^{3+}$)	885.3	32.59
	Ce $3d_{3/2}$ ($u'_0 = Ce^{3+}$)	903.8	40.28
$(PtO_x)_{0.25}(RuO_2-PbO_x)_{0.75}/C$	$Pt4f_{7/2}$ (Pt^0)	71.8	29.23
	$Pt4f_{5/2}$ (Pt^0)	74.9	20.28
	$Pt4f_{7/2}$ (Pt^{2+})	73.3	13.21
	$Pt4f_{5/2}$ (Pt^{2+})	76.6	20.76
	$Pt4f_{7/2}$ (Pt^{4+})	75.4	9.74
	$Pt4f_{5/2}$ (Pt^{4+})	78.7	6.26
$(PtO_x)_{0.25}(RuO_2-PbO_x)_{0.75}/C$	$Pb4f_{7/2}$ ($Pb^{2+} + Pb^{4+}$)	138.3	29.50
	$Pb4f_{5/2}$ ($Pb^{2+} + Pb^{4+}$)	143.1	23.51
	$Pb4f_{7/2}$ (Pb^{2+})	139.9	15.43
	$Pb4f_{5/2}$ (Pb^{2+})	144.7	13.82
	$Pb4f_{7/2}$ (Pb^{4+})	138.0	10.05
	$Pb4f_{5/2}$ (Pb^{4+})	143.0	7.69

Pb as a metal.[43,44] From the XPS studies, it is worthwhile mentioning that, in contrast to other methods for composite catalyst production (colloidal and reduction methods for instance),[45−47] the sol−gel method produces mainly metallic oxides.

Figure 3, presents X-ray diffractrograms (Cu Kα radiation) obtained for the ternary catalysts synthesized in this study. The measurements were compared to the crystallographic data of Joint Committee on Powder Diffraction Standards (JCPDS) of the possible components formed. Therefore, the structures found on the composites with their respective crystallographic file are the following: Pt (04-0802), PtO_2 (23-1306), Ru (06-0663), CeO_2 (43-1002), PbO_2 (45-1416), Pb_3O_4 (76-1799), MoO_3 (75-0912), Mo_4O_{11} (84-0687), Mo (01-1208), and $C_{(graphite)}$ (41-1887). On the graphics of Figure 3, symbols were used aiming to ease the identification of the diffractogram peaks.

The diffractrogram spectra of the ternary catalysts containing as third element Pb or Mo (panels B and C of Figure 3, respectively) show a slight indication of a possible Ru deposition in the metallic form, while in the catalysts containing Ce (Figure 3A), no peaks corresponding to the metallic Ru were observed.

On the other hand, according to the results obtained in the XRD analysis, the element Ce was deposited as dioxide (CeO_2). The deposition of molybdenum compounds as metallic Mo and oxide (MoO_3) was observed in XRD analyses; because the presence of only a peak related to Mo_4O_{11} was observed, their identification is incomplete and devious. The element Pb appears deposited mainly as lead tetroxide, Pb_3O_4, which is a mixture of oxides ($2PbO \cdot PbO_2$) and has a tetragonal crystal structure at room temperature. In the composites containing Pt−Pb, platinum is found in the metallic and oxidized forms, a fact that was not observed in other catalysts.

EDX analyses (Figure S1 in the Supporting Information) were used to estimate the elemental composition of the materials prepared by the sol−gel method. The results of these analyses are summarized in Table 2 and show a good agreement between the experimental and expected theoretical values for the catalysts containing cerium. However, the deposition of lead and molybdenum were apparently privileged with higher experimental composition values than the expected theoretical ones. Moreover, high-resolution EDX analysis (Table 2) taken together with the TEM measurements (Figure 4) and performed in a small area (100 nm^2) confirms these trends.

The values of particle sizes determined from the TEM images and their corresponding standard deviations are included in Table 2. The increase in the particle size in the lead-based electrocatalysts could be related to a higher oxidation of the platinum catalysts, as measured by XPS (PtO_x content). Furthermore, it is considerable that the catalyst containing the

(43) Mastelaro, V. R.; Lisboa-Filho, P. N.; Neves, P. P.; Schreiner, W. H.; Nascente, P. A. P.; Eiras, J. A. *J. Electron Spectrosc. Relat. Phenom.* **2007**, *156−158*, 476–481.
(44) Cao, H.; Wang, G.; Zhang, S.; Zhang, X. *Nanotechnology* **2006**, *17*, 3280–3287.
(45) Bönnemann, H.; Brinkmann, R.; Britz, P.; Endruschat, U.; Mörtel, R.; Paulus, U. A.; Feldmeyer, G. J.; Schmidt, T. J.; Gasteiger, H. A.; Behm, R. J. *J. New Mater. Electrochem. Syst.* **2000**, *3*, 199–206.
(46) Qian, Y.; Wen, W.; Adcock, P. A.; Jiang, Z.; Hakim, N.; Saha, M. S.; Mukerjee, S. *J. Phys. Chem. C* **2008**, *112*, 1146–1157.
(47) Shim, J.; Joung, K. Y.; Ahn, J. H.; Lee, W. M. *J. Electrochem. Soc.* **2007**, *154*, B165–B169.

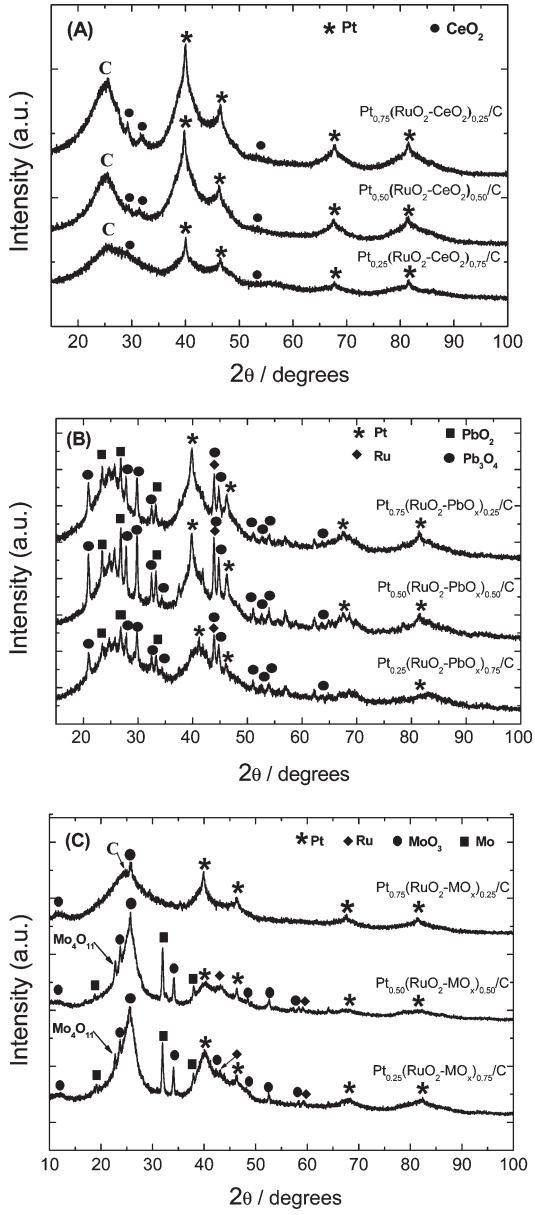

Figure 3. X-ray diffractograms of the composites of carbon powder modified by the ternary catalysts, with Cu Kα radiation and a continuous scan method.

highest content of lead formed agglomerates with higher particle sizes than both, with lower lead contents and the other catalysts without Pb. Thus, it seems that lead is deposited on the platinum nanoparticles forming cover layers, resulting in a slight increase in the particle size.

In addition to the determination of the particle sizes of the catalysts by microscopy techniques (TEM), the estimation of the average crystallite size of the deposited particles on the different materials was carried out considering the broadening of the diffraction reflections from the XRD patterns (Figure 3). For that, the Scherrer equation included in the Winfit 1.2 software[38] was used, and the results are also presented in Table 2. The average crystallite size of all of the prepared catalysts are in the same order of magnitude of the particle sizes, as expected. Thus and as previously reported,[28−31] these results show that the sol−gel method is an efficient and very appropriate technique to produce nanometric catalysts with crystallite sizes varying between 2.8 and 3.5 nm.

The electrochemical characterization of the composite electrodes was made by cyclic voltammetry at 5 mV s^{-1} in the supporting electrolyte (0.5 M H_2SO_4 aqueous solutions). The responses of the electrochemical characterization are presented in Figure 5. The electrochemical responses taken at the catalysts containing Pt−Ru−Ce (Figure 5A) show a significant inhibition of the surface electrochemical processes of platinum, like the hydrogen adsorption/desorption peaks. This is due to the incorporation of ruthenium and cerium, also leading in a noteworthy increase in the double-layer region because of an increase of the capacitive currents. Because of the high redox potential of CeO_2,[48] the Ru^{3+}−Ru^{4+} transition is favored, thus contributing to the increase in the currents.[49] Consequently, there is a direct relation between the increase in the pseudo-density currents and the increase in the Ru−Ce content of the composites.

Similarly, the blank responses of the catalysts containing Pt−Ru−Pb also show an increase in the pseudo-density currents because of the incorporation of ruthenium and lead oxides (Figure 5B). Again, the hydrogen adsorption/desorption processes on the platinum were inhibited because of the addition of the co-catalysts. The ternary catalysts containing Pt−Ru−Mo (Figure 5C) also present an increase in the capacitive current because of the incorporation of metallic oxides of Ru and Mo.

Hence, peaks in around 650 mV versus HESS corresponding to the transition of Ru^{3+}/Ru^{4+}[50] and peaks in 130, 320, and 690 mV versus HESS that can be due to the changes of the oxidation state of Mo, with their respective reduction peaks, are observed.[51] As in previous studies, the composites that present the highest amount of the combination Ru−Mo present the highest capacitive current.

3.2. Methanol Oxidation. Upon measurements made for the methanol oxidation by cyclic voltammetry (Figure 6), all of the onset potentials of the reaction were determined using a fixed current density of 10 A (g of Pt)$^{-1}$, except for the catalysts containing Pt−Ru−Mo, which were measured at 5 A (g of Pt)$^{-1}$, because these catalysts present a low current density in elevated potentials.

Upon Figure 6A, the electrodes $Pt_{0.25}(RuO_2{-}CeO_2)_{0.75}/C$ and $Pt_{0.50}(RuO_2{-}CeO_2)_{0.50}/C$ present the onset potential at ~375 mV and the electrode $Pt_{0.75}(RuO_2{-}CeO_2)_{0.25}/C$ presented the onset potential of oxidation at 570 mV. However, the $Pt_{0.50}(RuO_2{-}CeO_2)_{0.50}/C$ catalyst showed a higher current density in more positive potentials in comparison to the other catalysts.

The the presence of ruthenium oxide increases the capacitive currents of these catalysts in comparison to that observed on the $Pt_{0.50}{-}(CeO_2)_{0.50}/C$ catalyst in the methanol oxidation (Figure S2 in the Supporting Information). Similarly, the voltammetry obtained in these ternary catalysts presents a decrease in the reactivation current, because the ruthenium oxides apparently ease the oxidation of the intermediaries adsorbed during the oxidation of methanol.

In the catalyst containing Pb in its composition, although presenting similar current densities to the ones obtained on ternary catalysts containing Ce, the methanol oxidation begins

(48) De Faria, L. A.; Boodts, J. F. C.; Trasatti, S. *Electrochim. Acta* **1997**, *42*, 3525–3530.
(49) Santana, M. H. P.; Da Silva, L. M.; De Faria, L. A. *Electrochim. Acta* **2003**, *48*, 1885–1891.
(50) Mattos-Costa, F. I.; De Lima-Neto, P.; Machado, S. A. S.; Avaca, L. A. *Electrochim. Acta* **2003**, *44*, 1515–1523.
(51) Ordóñez, L. C.; Roquero, P.; Sebastian, P. J.; Ramírez, J. *Catal. Today* **2005**, *107−108*, 46–52.

Table 2. Chemical Analysis of the Sol−Gel-Prepared Catalysts from EDX Measurements, with the Crystallite Size Calculated from XRD Analysis Using the WinFit 1.2 Program and the Particle Size Calculated from TEM

composite	EDX composition (atomic %)	high-resolution EDX (atomic %)	expected composition (atomic %)	particle size TEM (nm)	crystallite size (nm)[a]
$Pt_{0.25}(RuO_2-CeO_2)_{0.75}/C$	28:35:37	26:36:38	25:37.5:37.5	3.0 ± 1.7	2.9
$Pt_{0.50}(RuO_2-CeO_2)_{0.50}/C$	47:26:27	48:24:28	50:25:25	3.0 ± 1.6	2.9
$Pt_{0.75}(RuO_2-CeO_2)_{0.25}/C$	76:11:13	73:14:12	75:12.5:12.5	2.8 ± 0.8	2.8
$(PtO_x)_{0.25}(RuO_2-PbO_x)_{0.75}/C$	23:30:42	23:24:53	25:37.5:37.5	4.2 ± 1.6	3.5
$(PtO_x)_{0.50}(RuO_2-PbO_x)_{0.50}/C$	47:21:32	46:26:28	50:25:25	4.1 ± 1.2	3.1
$(PtO_x)_{0.75}(RuO_2-PbO_x)_{0.25}/C$	60:17:23	38:28:34	75:12.5:12.5	4.0 ± 1.7	3.0
$Pt_{0.25}(RuO_2-MoO_3)_{0.75}/C$	22:32:46	23:34:43	25:37.5:37.5	3.0 ± 1.6	2.9
$Pt_{0.50}(RuO_2-MoO_3)_{0.50}/C$	41:24:35	43:23:34	50:25:25	3.1 ± 1.2	3.0
$Pt_{0.75}(RuO_2-MoO_3)_{0.25}/C$	64:13:23	66:14:20	75:12.5:12.5	3.0 ± 0.9	3.1

[a] Calculated using the WinFit 1.2 program.

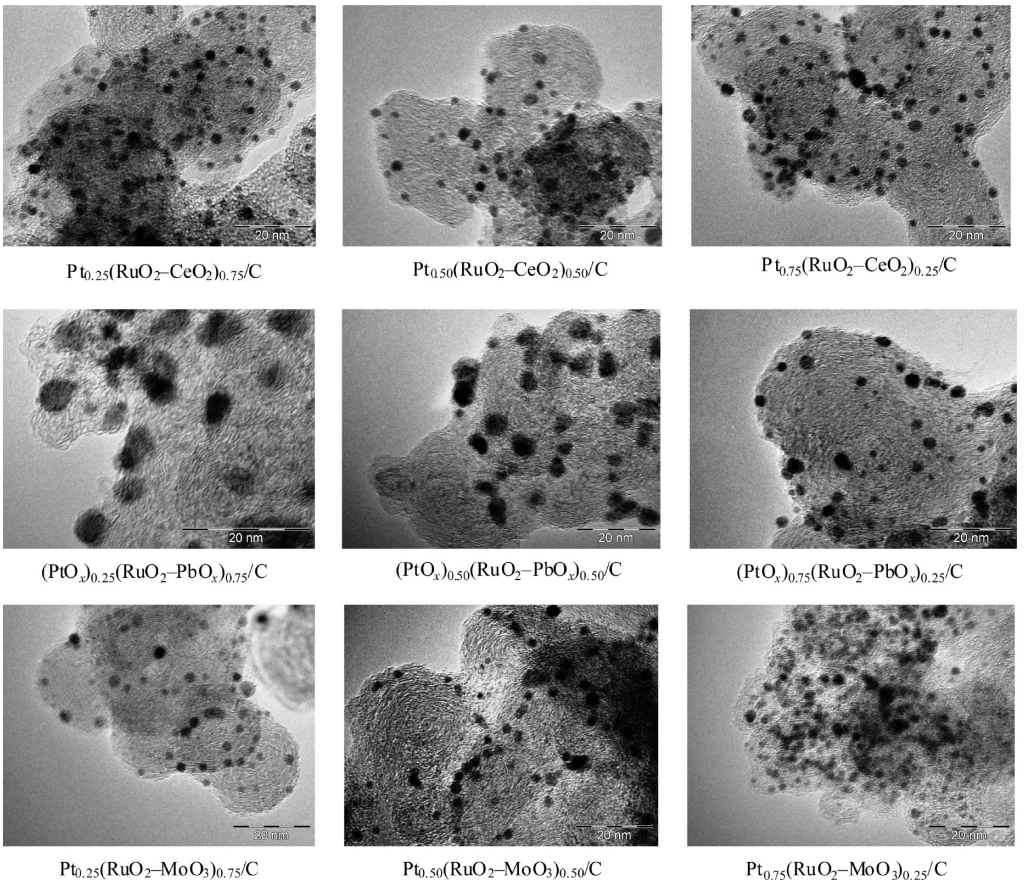

Figure 4. TEM micrographs obtained on the ternary composites prepared by the sol−gel method.

at ∼490 mV on the $(PtO_x)_{0.25}(RuO_2-PbO_x)_{0.75}/C$ catalyst and on ∼540 mV in both the $(PtO_x)_{0.50}(RuO_2-PbO_x)_{0.50}/C$ and $(PtO_x)_{0.75}(RuO_2-PbO_x)_{0.25}/C$ catalysts, as shown in Figure 6B. It is possible to note that the catalyst that contains higher amounts of the combination Ru−Pb presents the best catalytic performance as well as the absence of the reactivation current, which is due to the oxidation of intermediaries adsorbed in the reduced surface of Pt in the backward scan. This indicates that the oxidation of methanol in this catalytic composite is direct without the formation of intermediaries strongly adsorbed, as discussed hereafter.

The voltammetric techniques have outcomes of difficult comparison. Hence, for a more elaborated analysis and aiming to understand the behavior of different composites for methanol oxidation in the stationary state, polarization curves were made in quasi-steady state (Tafel plots). Figure 7 presents the Tafel plot obtained for methanol oxidation in acid medium on the ternary catalysts, which is the best performance obtained for the methanol oxidation reaction. The onset of the methanol oxidation was determined at 0.07 A (g of Pt)$^{-1}$.

The $Pt_{0.50}(RuO_2-CeO_2)_{0.50}/C$ catalyst stood out among the ternary catalysts of Ce, presenting the onset potential of methanol oxidation at around 277 mV, reducing in ∼209 mV the potential in comparison to a commercial Pt/C, as observed in Table 3, and the current density measured at 450 mV was about 140 times higher than the commercial Pt and 11 times higher than the commercial Pt−Ru catalyst. Interesting results were also showed by the $Pt_{0.25}(RuO_2-CeO_2)_{0.75}/C$ catalyst, with an onset potential of 302 mV.

In cases of catalysts containing lead, the $Pt_{0.25}(RuO_2-PbO_x)_{0.75}/C$ catalyst presented a catalytic performance 8 times higher than that presented by the Pt−Ru/C catalyst of E-Tek, Inc. Nevertheless, in comparison to Pt/C from E-Tek, Inc., this lead-based catalyst presented a reduction of the onset potential of 184 mV to lower potentials, which conduces to a catalytic performance 106 times higher than that presented

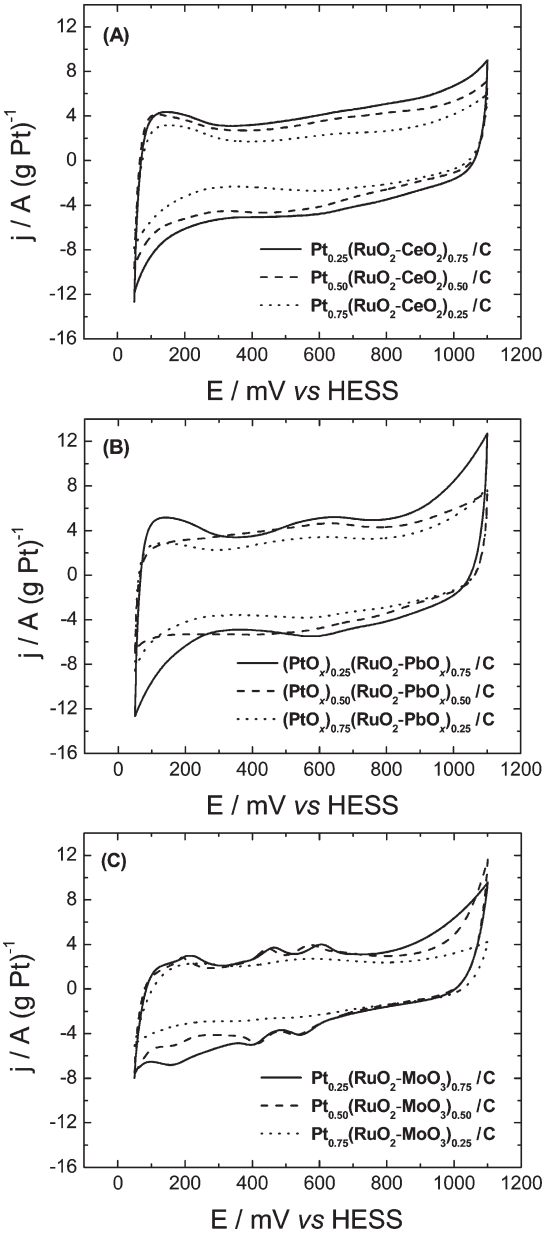

Figure 5. Cyclic voltammograms (second cycle) made on the ternary composites prepared by the sol−gel method on the support electrolyte (0.5 M H_2SO_4) at $\nu = 5$ mV s^{-1}.

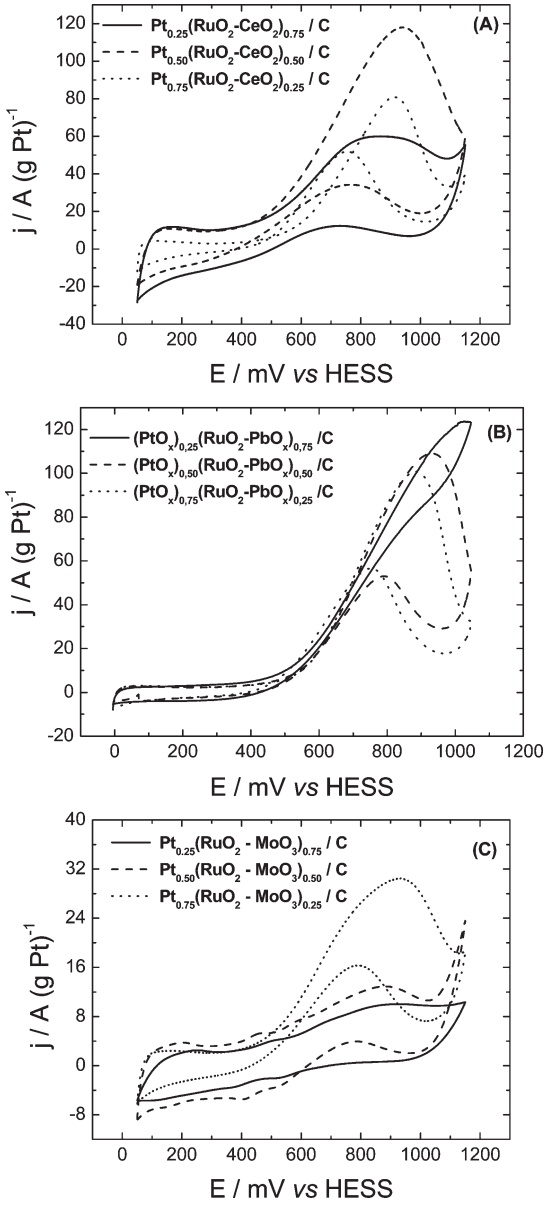

Figure 6. Cyclic voltammograms (second cycle) of electrochemical oxidation of methanol (0.5 M) on the ternary catalysts prepared by the sol−gel method in acid medium (0.5 M H_2SO_4) were taken at $\nu = 5$ mV s^{-1}.

by the Pt/C catalyst. In addition, the $Pt_{0.25}(RuO_2-PbO_x)_{0.75}/C$ catalyst displayed the highest catalytic activity for the methanol oxidation in acid medium among all of the catalysts containing lead.

Although elevated catalytic activity for methanol oxidation was observed in a previous publication using a catalyst prepared by the sol−gel method and using a fixed proportion of metals (50% Pt, 25% Ru, and 25% Pb) on Vulcan XC-72R carbon powder.[27] This study shows that the catalytic activity for methanol oxidation under this ternary catalyst is favored by high proportions or element amounts of Ru and Pb, as observed in Figures 6 and 7.

In Figure 7, it is shown that the onset potential of methanol oxidation over the $Pt_{0.75}(RuO_2-MoO_3)_{0.25}/C$ catalyst is around 293 mV. This value is almost 190 mV lower than that presented by pure Pt and 75 mV lower than that obtained on $Pt_{0.75}-Ru_{0.25}/C$ from E-Tek, Inc. This reduction on the onset potential of the oxidation reaction leads to current density values of about 8 and 111 times higher than both the $Pt_{0.75}-Ru_{0.25}/C$ and Pt/C catalysts, from E-Tek, Inc., respectively. It is worth mentioning that the catalytic activity of this catalyst was slightly lower than that observed at the $Pt_{0.50}(RuO_2-CeO_2)_{0.50}/C$ composite (1.3 times lower current density; see Table 3).

Another important technique for the study of catalytic activities and superficial stability of the catalysts is the use of chronoamperometry. The current density−time curves presented in Figure 8 were made on the ternary catalysts that presented the best performance for the electrochemical oxidation of methanol in acid medium for each group of catalysts prepared in this study. For such, the potential was established at 500 mV versus HESS, and the chronoamperometric tests were made for 1 h.

As can be seen in Figure 8, the $Pt_{0.50}(RuO_2-CeO_2)_{0.50}/C$ catalyst is poisoned in a smaller degree if compared to others,

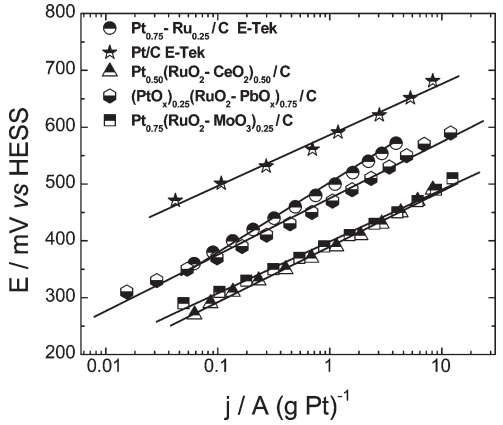

Figure 7. Tafel plots for 0.5 M methanol electrochemical oxidation in acid medium (0.5 M H_2SO_4) obtained under the best ternary electrodes in each group studied. All of the data were obtained on the basis of the values of the potentiostatic current measured after 300 s of polarization every 20 mV.

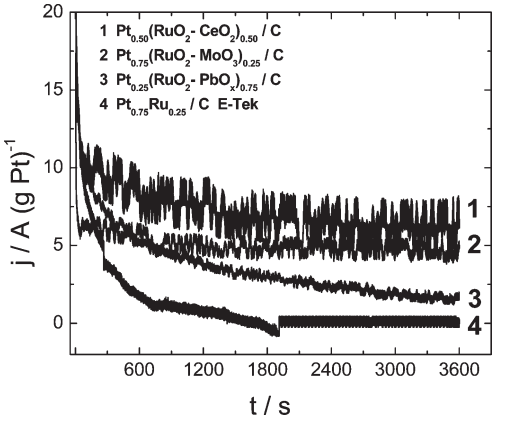

Figure 8. Variation of the normalized current by mass of Pt with time at a constant potential (500 mV versus HESS) for oxidation of 0.5 M methanol in acid medium (0.5 M H_2SO_4) made regarding the best ternary catalysts in each group and the commercial catalyst $Pt_{0.75}-Ru_{0.25}/C$ from E-Tek, Inc.

Table 3. Parameters Obtained from the Electrochemical Experiments in Quasi-steady State (Tafel Plots) for All Catalysts Studied

catalyst	onset potential taken at 0.07 A (g of Pt)$^{-1}$ (mV versus HESS)	pseudo-current density determined at 450 mV [A (g of Pt)$^{-1}$]
Pt/C from E-Tek, Inc.	486	0.03
$Pt_{0.75}-Ru_{0.25}$/C from E-Tek, Inc.	369	0.38
$Pt_{0.25}(RuO_2-CeO_2)_{0.75}/C$	302	4.12
$Pt_{0.50}(RuO_2-CeO_2)_{0.50}/C$	277	4.20
$Pt_{0.75}(RuO_2-CeO_2)_{0.25}/C$	306	1.11
$(PtO_x)_{0.25}(RuO_2-PbO_x)_{0.75}/C$	302	3.18
$(PtO_x)_{0.50}(RuO_2-PbO_x)_{0.50}/C$	348	0.74
$(PtO_x)_{0.75}(RuO_2-PbO_x)_{0.25}/C$	359	0.58
$Pt_{0.25}(RuO_2-MoO_x)_{0.75}/C$	432	0.11
$Pt_{0.50}(RuO_2-MoO_x)_{0.50}/C$	369	0.37
$Pt_{0.75}(RuO_2-MoO_x)_{0.25}/C$	293	3.34

in this applied potential (500 mV), because it presents a higher pseudo-current density and a relatively slow decay. The fact that the presence of high values of current density is presented by the catalysts containing Pt−Ru−Ce in low potentials is a very important feature in application of fuel cells, because it allows a better use of the energy cell. On the other hand, the $(PtO_x)_{0.25}(RuO_2-PbO_x)_{0.75}/C$ catalyst is apparently poisoned much faster than other ternary composites but presents higher current densities than the $Pt_{0.75}-Ru_{0.25}/C$ catalyst from E-Tek, Inc.

During the chronoamperometric tests shown in Figure 8, a sample was taken (0.5 mL) from the solution after 60 min for the HPLC analyses that will be described furthermore. This was made for the ternary catalysts, which presented the best catalytic performance, and commercial $Pt_{0.75}-Ru_{0.25}/C$ from E-Tek, Inc.

4. Discussion

The diffractrogram spectra of the ternary catalysts do not show the presence of crystalline ruthenium compounds, indicating that this element was deposited as oxides in the amorphous form, because clear and well-defined signals of ruthenium oxides were observed in the XPS measurements.

In this context, amorphous RuO_2 powders were already synthesized by the sol−gel method as the active electrode material for electrochemical capacitors[52] and by other techniques, such as spraying of solutions of $RuCl_3$ for the preparation of RuO_2 films deposited on indium tin oxide (ITO) substrates.[53] The characterization of Pt/Ru/Ni alloy nanoparticles, prepared for the study of the methanol electro-oxidation in acid media, also showed the presence of amorphous RuO_2 and RuO_3 by XPS measurements.[54] Similar to our case, no peaks for crystalline Ru or ruthenium oxides were observed in the XRD analyses, demonstrating the amorphous character of the Ru compounds in this alloy catalyst synthesized at room temperature using a conventional reduction method with $NaBH_4$. These authors also concluded that the oxides function as the oxygen donors for the oxidation process (surface CO removal), and as a result, their catalysts had excellent catalytic activity compared to pure Pt.

On the other hand, XRD analysis showed the deposition of CeO_2, which is in agreement with the XPS results. For the deposition of molybdenum compounds, metallic Mo and oxide (MoO_3) were observed in XRD analyses; because the presence of only a peak related to Mo_4O_{11} was observed, their identification is incomplete and misleading. In this manner, because the XPS analyses showed that Mo was deposited as Mo^0 and to a great extent in the oxidation state 6+, it was mainly deposited as crystalline orthorhombic MoO_3 (JCPDS 75-0912). The deposition of Pb mainly as lead tetroxide, Pb_3O_4, is in agreement with the preferential oxidation state observed in XPS measurements and related to the Pb_3O_4 compound.

It is worthwhile noting that the composites containing Pt−Pb are particular cases and differ from others already studied; hence, on the basis of the analyses of XPS made, the platinum is found in the metallic and oxidized forms, a fact that was not observed in other catalysts where only metallic Pt was observed. This higher oxidation of Pt could be related to the low melting point of lead (mp = 328 °C) because, during the thermal treatment at 400 °C, lead is still in the liquid state, favoring the formation of platinum oxides. However, this phenomenon needs further investigation.

On the other hand, it is clear from the TEM studies that particle sizes observed for the catalyst are small and well-controlled

(52) Zheng, J. P.; Jow, T. R. *J. Power Sources* **1996**, *62*, 155–159.

(53) Gujar, T. P.; Shinde, V. R.; Lokhande, C. D.; Kim, W.-Y.; Jung, K.-D.; Joo, O.-S. *Electrochem. Commun.* **2007**, *9*, 504–510.

(54) Park, K.-W.; Choi, J.-H.; Kwon, B.-K.; Lee, S.-A.; Sung, Y.-E.; Ha, H.-Y.; Hong, S.-A.; Kim, H.; Wieckowski, A. *J. Phys. Chem. B* **2002**, *106*, 1869–1877.

in the range between 2.8 and 4.2 nm. Because the particle size of the platinum nanoparticles, determined by TEM, is 2.4 nm, it seems that the atoms of the co-catalyst were deposited on the platinum particles, resulting in a small increase of the particle catalyst sizes. Because the particle sizes of the ternary catalysts are similar for the different compositions, it can be stated that the differences observed for the catalytic activity of these materials (see later) could be mainly due to their compositions, thus revealing a real catalytic effect.

Similarly, the crystallite size, determined from XRD measurements, of the Pt nanoparticles before deposition was 2.4 nm, and for the ternary catalysts, it was between 2.8 and 3.5 nm; this also suggests the deposition of the co-catalysts in close contact with the Pt nanoparticles, which is very positive for the occurrence of the bifunctional mechanism in the ternary catalyst.

Upon the electrochemical experiments to compare the catalytic activity of the prepared catalysts toward methanol oxidation, it is worthwhile noting that the enhanced catalytic activity of the $Pt_{0.50}(RuO_2-CeO_2)_{0.50}/C$ composite electrode (Figure 6A) is observed initially as a very low value of the onset potential [277 mV versus HESS, measured at 10 A (g of Pt)$^{-1}$]. This value is lower than the ones obtained at several ternary catalysts in voltammetric curves and steady-state polarization experiments, i.e., for instance, 324 mV at carbon-nanotube-supported Pt−Ru−Ni determined using linear sweep voltammetry,[55] 550 mV at Pt−Ni−Pb/C ternary alloy catalysts determined using cyclic voltammetry,[56] and ∼415 mV at $Pt_{0.472}Ru_{0.413}Sn_{0.115}/C$ catalyst determined using Tafel plots.[57]

This relevant improvement in the catalytic activity of this ternary catalyst can be related to various factors, primarily, the bifunctional mechanism[58] present in the Pt−Ru alloys, the electronic effect induced by Ru on the nearby Pt atoms (ligand effect),[59] or both;[60] on the other hand, it is also likely as a result of the removal of the intermediary CO on the Pt surface during the oxidation process,[61] because the reduced form of cerium (at low potentials) apparently promotes the formation of highly reactive anionic radicals O_2^-,[61] which are very efficient for the CO oxidation.

In this sense, two proposed mechanisms have been idealized to explain the enhanced catalytic activity toward methanol oxidation observed on Pt/CeO_2 composites, by either inhibiting CO adsorption or the oxygen storage capacity of ceria playing a role to ease the oxidation of adsorbed CO.[13] It has also been reported that CeO_2 supported on Pt particles possesses a large electrochemically active surface area for methanol electrooxidation because CeO_2 can release oxygen reversibly.[12]

Wang and co-workers[62] studied the electrochemical oxidation of methanol in the $Pt-CeO_2$ catalyst supported in carbon nanotubes ($Pt-CeO_2$/CNTs). This catalyst presented the highest catalytic activity for methanol oxidation when compared to Pt also supported in carbon nanotubes, and the dissolution potential of CO changed to several less positive values, indicating that CeO_2 facilitates the CO oxidation and, therefore, the methanol oxidation. Also, Guo et al.[63] studied the oxidation of methanol in the catalyst containing $Pt-Ru-CeO_2/C$ (synthesized by the sodium borohydride reduction method) in acid medium using linear voltammetry and chronoamperometry. The results showed that the $Pt-Ru_{0.7}(CeO_2)_{0.3}/C$ catalyst presented a higher methanol oxidation current than the Pt−Ru/C catalyst. Moreover, the use of nanoscale ceria particles incorporated on a Pt composite (Pt/CeO_2), as a novel anode material for the direct oxidation of methanol, have shown enhanced catalytic activity,[13] which is presumably due to the oxygen capture and release capacity of ceria.

On the other hand, good results for electrochemical oxidation of methanol have been obtained by the combination of Pt with oxophilic elements, such as Ru, Sn, and Mo,[58,64−66] which promote the electro-dissociation of water at lower positive potentials than Pt. Specifically, the intermediary change of the oxidation states of Mo (Mo^{III} and Mo^{IV}) works as OH^- donors for Pt.[51] Besides that, Mo demonstrated having a lower affinity with CO;[67] therefore, more superficial sites of Mo can be available in a wide range of potentials for water dissociation and contributing in this sense to the generation of OH^- species that oxidize organic intermediaries adsorbed over the nearby Pt sites. The calculation of Pt d-orbital vacancy for both Pt−Ru and Pt−Mo have indicated that Mo is more easily oxidizable than Ru, which, in turn, is a favorable situation for the oxidation of CO adsorbed on the Pt surface, which is produced by methanol oxidation.[16] These facts can explain the good performance of ternary catalysts containing Mo for the methanol oxidation (see Table 3).

The onset potential of methanol oxidation measured at 5 A (g of Pt)$^{-1}$ on the catalyst containing Pt−Ru−Mo (Figure 6C) was around 500 mV for $Pt_{0.75}(RuO_2-MoO_3)_{0.25}/C$, 525 mV for $Pt_{0.50}(RuO_2-MoO_3)_{0.50}/C$, and 600 mV for $Pt_{0.25}(RuO_2-MoO_3)_{0.75}/C$. Different from that observed up to now for the ternary catalysts, the best catalytic performance was observed for the catalyst containing the highest amount of Pt in comparison to the combination Ru−Mo [$Pt_{0.75}(RuO_2-MoO_3)_{0.25}/C$]. This can be due to the fact that, in the catalyst with lower amounts of Pt, there is an excess of oxygenated species in low potentials supplied by the Ru and Mo oxides, limiting the number of free active sites of Pt, which are necessary for the absorption and dissociation of the methanol molecule.

It is worthwhile mentioning as well, as observed in the EDX analyses, that Mo was deposited preferably (see Table 2), and in this manner, Mo can be covering Pt sites, reducing the amount of the exposed area of Pt.

In cases of catalysts containing lead in Figure 6B, the $Pt_{0.25}(RuO_2-PbO_x)_{0.75}/C$ catalyst presented the highest catalytic activity for the methanol oxidation in acid medium among all of the catalysts containing lead, which is also higher than that obtained by the Pt/C and Pt−Ru/C catalysts of E-Tek, Inc. Although elevated catalytic activity for methanol oxidation was observed in a previous publication using a catalyst prepared by the sol−gel method and using a fixed

(55) Ye, F.; Chen, S.; Dong, X.; Lin, W. *J. Nat. Gas Chem.* **2007**, *16*, 162–166.
(56) Chen, M.; Wang, Z.; Ding, Y.; Yin, G. *Electrochem. Commun.* **2008**, *10*, 443–446.
(57) Zhu, J.; Cheng, F.; Tao, Z.; Chen, J. *J. Phys. Chem. C* **2008**, *112*, 6337–6345.
(58) Watanabe, M.; Motoo, S. *J. Electroanal. Chem.* **1975**, *60*, 267–273.
(59) Janssen, M. M. P.; Moolhuysen, J. *J. Catal.* **1977**, *46*, 289–296.
(60) Krausa, M.; Vielstich, W. *J. Electroanal. Chem.* **1994**, *379*, 307–314.
(61) Campos, L. C.; Roldán, C.; Aponte, M.; Ishiwaka, Y.; Cabrera, C. R. *J. Electroanal. Chem.* **2005**, *581*, 206–215.
(62) Wang, J.; Xi, J.; Bai, Y.; Shen, Y.; Sunc, J.; Chena, L.; Zhua, W.; Qiu, X. *J. Power Sources* **2007**, *164*, 555–560.
(63) Guo, J. W.; Zhao, T. S.; Prabhuram, J.; Chen, R.; Won, C. W. *J. Power Sources* **2006**, *156*, 345–354.
(64) Gotz, M.; Wendt, H. *Electrochim. Acta* **1998**, *43*, 3637–3644.
(65) Frelink, T.; Visscher, W.; Van Veen, J. *Surf. Sci.* **1995**, *335*, 353–360.
(66) Watanabe, M.; Motoo, S. J. *J. Electroanal. Chem.* **1975**, *60*, 275–283.
(67) Mukerjee, S.; Urian, R. C. *Electrochim. Acta* **2002**, *47*, 3219–3231.

proportion of metals (50% Pt, 25% Ru, and 25% Pb) on Vulcan XC-72R carbon powder.[27] This study shows that the catalytic activity for methanol oxidation under this ternary catalyst is favored by high proportions or elemental amounts of Ru and Pb, as observed in Figures 6 and 7.

It should be noted at this point that the performance of the composite obtained by the sol−gel method is mainly dependent upon the catalytic activity and not a size effect of the particle, as reported previously by Suffredini et al.[27] and observed in Figure 4 and Table 2, where the particle sizes of all catalysts vary randomly between 2.8 and 4.2 nm and do not present a tendency that agrees with the catalytic activity observed in the experiments of cyclic voltammetry and the Tafel plots discussed until this point.

From the mechanistic point of view, it is known that methanol absorption occurs in various stages, forming different species because of the partitioning of the hydrogen atom bonds from the methanol molecule

$$CH_3OH \rightarrow \underset{x}{CH_2OH} + H + e^- \rightarrow \underset{xx}{CHOH} + H + e^- \rightarrow \underset{xxx}{COH} + H + e^- \rightarrow \underset{x}{CO} + H + e^- \quad (1)$$

where x means a site for Pt.[68] As can be observed in the previous reaction, the successive dissociation of the C−H bond to form CO_{ads} requires the availability of several neighboring sites of Pt. CO_{ads} can therefore react with an adsorbed oxygen donor, for example, OH_{ads}, following the Langmuir−Hinshelwood mechanism.

$$CO_{ad} + OH_{ad} \rightarrow CO_2 + H^+ + e^- \quad (2)$$

However, it was also shown that the methanol molecule could be adsorbed via the oxygen atom, forming the methoxide (H_3CO) intermediary, and thus, formaldehyde and formic acid can be formed from the intermediaries H_3CO and CHOH, respectively.[68−70] These species diffuse to the bulk of the solution, resulting in a loss of potential because of the loss of charge by the methanol molecule.

$$CH_3OH \rightarrow \underset{x}{H_3CO} + H^+ + e^- \rightarrow \underset{x}{HCHO} + H^+ + e^- \quad (3)$$

$$\underset{x}{HCHO} + H_2O \rightarrow HCOOH + 2H^+ + 2e^- \quad (4)$$

$$HCOOH \rightarrow CO_2 + 2H^+ + 2e^- \quad (5)$$

Hence, the formation of formic acid and formaldehyde was identified using high-performance liquid chromatography (HPLC) with two types of detectors, a refractive index detector for the detection of formaldehyde and an ultraviolet (UV) detector to detect the formic acid, using a system already reported in the literature.[70,71]

In Table 4, the concentration values of formaldehyde and formic acid formed during the chronoamperometric tests can be seen, as well as the charge values that were found in these tests. It should be mentioned that the charge that varied during the chronoamperometric tests (Table 4) correspond to a small fraction of methanol consumed in the reaction.

Table 4. Concentration Values of Formaldehyde and Formic Acid after 60 min of Application of 500 mV of Potential and Charge Values Obtained from the Chronoamperometric Curves (Figure 8)

catalyst	formaldehyde (mM)	formic acid (mM)	charge (C)
$Pt_{0.50}(RuO_2-CeO_2)_{0.50}/C$	0.04	0.05	24.30
$Pt_{0.75}(RuO_2-MoO_3)_{0.25}/C$	0.05	0.05	16.36
$(PtO_x)_{0.25}(RuO_2-PbO_x)_{0.75}/C$	0.21	0.19	11.40
$Pt_{0.75}-Ru_{0.25}/C$ from E-Tek, Inc.	0.24	0.21	3.50

Therefore, these results indicate that, on $Pt_{0.50}(RuO_2-CeO_2)_{0.50}/C$ and $Pt_{0.75}(RuO_2-MoO_3)_{0.25}/C$ catalysts (which present higher charge values and a low production of formaldehyde and formic acid), the efficiency of the methanol oxidation is higher and likely conducted preferably by the pathway that produces CO_2 passing through the intermediate CO_{ads} (reactions 1 and 2).

These observations are in accordance with the electrochemical results obtained on the Tafel plots and in the current−time curves (see Figures 7 and 8) that show that the catalytic activity for methanol oxidation presented by the $Pt_{0.50}(RuO_2-CeO_2)_{0.50}/C$ and $Pt_{0.75}(RuO_2-MoO_3)_{0.25}/C$ catalysts is higher than those presented by the $Pt_{0.75}-Ru_{0.25}/C$ catalyst from E-Tek, Inc. and the $(PtO_x)_{0.25}(RuO_2-PbO_x)_{0.75}/C$ catalyst, with a larger emphasis for the $Pt_{0.50}(RuO_2-CeO_2)_{0.50}/C$ catalyst.

5. Conclusions

This study describes the preparation of ternary composites containing $Pt_x-(RuO_2-M)_{1-x}/C$ (where M represents CeO_2, MoO_3, or PbO_x) by the sol−gel method from Pt/C (from E-Tek, Inc.) commercial catalysts. The effect of catalyst composition on the methanol electro-oxidation in acid media was also studied using electrochemical and chromatographic techniques. TEM measurements and the analyses of the spectra from XRD indicated that the catalysts were deposited as nanoparticles in the range of 2.8−4.2 nm in diameter. In addition, EDX, XRD, and XPS measurements demonstrated the successful deposition of the co-catalysts on the Pt/C as metallic oxides (RuO_2, CeO_2, PbO_x, and MoO_3).

Cyclic voltammetry, quasi-steady-state polarization curves, and chronoamperometric tests showed that the $Pt_{0.50}(RuO_2-CeO_2)_{0.50}/C$ composite displays the highest catalytic activity toward the methanol oxidation reaction among all ternary catalyst prepared here. The onset potential of the methanol oxidation reaction was shifted at 207 and 91 mV to lower positive potentials than those observed for the Pt/C and $Pt_{0.75}-Ru_{0.25}/C$ commercial catalysts, respectively. As a consequence, the current densities taken at 450 mV were 140 and 11 times higher than those at Pt/C and $Pt_{0.75}-Ru_{0.25}/C$ (from E-Tek, Inc.), respectively. The $Pt_{0.25}(RuO_2-CeO_2)_{0.75}/C$ and $Pt_{0.75}(RuO_2-MoO_3)_{0.25}/C$ composites also deserve attention because they similarly showed high catalytic activity toward the methanol oxidation reaction.

In addition, the $Pt_{0.50}(RuO_2-CeO_2)_{0.50}/C$ composite produced the lowest quantity of formic acid and formaldehyde and presented the highest electrochemical charge in chronoamperometric experiments when compared to the other ternary homemade catalysts and a commercially available $Pt_{0.75}-Ru_{0.25}/C$ composite (from E-Tek, Inc.). Chromatographic observations suggest that the oxidation of methanol occurs mainly by a pathway that produces CO_2 forming intermediary CO_{ads}. This fact is important because formic acid and

(68) Bagotzki, V. S.; Vassiliev, Y. B.; Khazova, O. A. *J. Electroanal. Chem.* **1977**, *81*, 229–238.
(69) Ota, K.-I.; Nakagawa, Y.; Takahashi, M. *J. Electroanal. Chem.* **1984**, *179*, 179–186.
(70) Batista, E. A.; Malpass, G. R. P.; Motheo, A. J.; Iwasita, T. *Electrochem. Commun.* **2003**, *5*, 843–846.
(71) Batista, E. A.; Malpass, G. R. P.; Motheo, A. J.; Iwasita, T. *J. Electroanal. Chem.* **2004**, *571*, 273–282.

formaldehyde formed during the methanol oxidation diffusing to the bulk solution resulted in a loss of power, as a result of the loss of charge per molecule of methanol. Thus, from the quaternary catalysts studied, the $Pt_{0.50}(RuO_2-CeO_2)_{0.50}/C$, $Pt_{0.25}(RuO_2-CeO_2)_{0.75}/C$, $Pt_{0.75}(RuO_2-MoO_3)_{0.25}/C$, and $(PtO_x)_{0.25}(RuO_2-PbO_x)_{0.75}/C$ ternary catalysts are promising materials for practical applications to be used as anodes in fuel cell systems and deserve future investigations.

Acknowledgment. The authors thank the National Council of Technological and Scientific Development (CNPq, processes 141421/2004-5 and 304018/2009-0) from Brazil for the scholarships and financial support of this work. We are also grateful to Prof. Peter Hammer from Universidade Estadual Paulista (UNESP) for his contribution in the XPS analyses.

Supporting Information Available: EDX spectra taken on the ternary composites prepared by the sol−gel method (Figure S1) and cyclic voltammetry curve (second cycle) of electrochemical oxidation of methanol (0.5 M) at the $Pt_{0.50}-(CeO_2)_{0.50}/C$ catalyst prepared by the sol−gel method in acid medium (0.5 M H_2SO_4), taken at $\nu = 5$ mV s^{-1} (Figure S2). This material is available free of charge via the Internet at http://pubs.acs.org.